machines

MDPI

Article

Enhancing Spraying Performance with Active Stability Control in Multi-Link Mechanisms

Naiyu Shi [1,2], He Li [3,*], Yongkang Yang [1], Hongliang Hua [1], Junhong Ye [1], Zheng Chen [1] and Ting Xu [1]

[1] School of Mechanical Engineering, Changzhou Institute of Technology, Changzhou 213032, China; shiny@czust.edu.cn (N.S.); 22010433@czust.edu.cn (Y.Y.); huahl@czu.cn (H.H.); 22010434@czust.edu.cn (J.Y.); 22010105@czust.edu.cn (Z.C.); 23010625@czust.edu.cn (T.X.)
[2] School of Automotive and Traffic Engineering, Jiangsu University, Zhenjiang 212013, China
[3] School of Sciences, Changzhou Institute of Technology, Changzhou 213032, China
* Correspondence: lihe@czust.edu.cn

Abstract: This study proposes an active stability control method for the multi-link mechanism of spraying equipment to enhance its spraying performance. Traditional spraying operations typically focus on protecting only the tops of crops, whereas the multi-link mechanism can adjust the angle and position of the nozzles in coordination, achieving comprehensive protection for the crops. However, the characteristic of uneven output speed in the multi-link mechanism results in variations in the spraying amount at different positions. To address this issue, this study developed a method for actively adjusting the stability of the output end speed. First, a differential equation was established to relate the input speed to the output speed using vector methods, implicit function transformation to explicit functions, and regression analysis. The feasibility of this method was verified through simulations using MATLAB Simulink R2018a and Adams 2018. Prototype test results indicate that this speed adjustment method improved the stability of the output angular velocity, reducing the coverage rate variation between the upward, sideways, and downward of the leaves by 12.53% during the spraying process. Therefore, the method proposed in this study can enhance the uniformity of spraying, further improving the utilization of pesticides, which is beneficial for the green ecological sustainable development in the agricultural field. Additionally, this control method is also applicable to other types of link mechanisms, providing a reference for improving the output stability of link mechanisms.

Keywords: linkage mechanism; active regulation; Simulink; spraying machine

check for updates

Academic Editor: Shaoping Bai

Received: 22 December 2024
Revised: 24 January 2025
Accepted: 26 January 2025
Published: 28 January 2025

Citation: Shi, N.; Li, H.; Yang, Y.; Hua, H.; Ye, J.; Chen, Z.; Xu, T. Enhancing Spraying Performance with Active Stability Control in Multi-Link Mechanisms. *Machines* **2025**, *13*, 104. https://doi.org/10.3390/machines13020104

Copyright: © 2025 by the authors. Licensee MDPI, Basel, Switzerland. This article is an open access article distributed under the terms and conditions of the Creative Commons Attribution (CC BY) license (https://creativecommons.org/licenses/by/4.0/).

1. Introduction

The application of pesticides is essential for the growth and development of agricultural crops. With the advancement of various technological innovations, the methods for pesticide application have evolved significantly, transitioning from traditional backpack sprayers to modern robotic sprayers [1,2]. Conventional pesticide application techniques typically utilize a blanket spraying method that employs high volumes of chemicals to enhance efficacy. In contrast, contemporary advancements in spraying technology primarily focus on pesticide conservation and application precision [3,4]. To improve pesticide efficiency, protect the environment, and ensure accurate delivery, researchers have developed a range of spraying devices and methodologies. These innovations include electrostatic pesticide spraying [5], air-assisted spraying technology [6], machine learning-driven targeted spraying systems [7], and adjustable linkage mechanisms [8,9]. Electrostatic pesticide

spraying technology utilizes the principle of electrostatic adsorption to enhance the deposition rate of droplets, thereby improving their adherence to crop surfaces [10]. The air-assisted spray technology utilizes forced airflow to manipulate the structure of crop leaves, thereby enhancing the penetration of droplets into the inner layers of the vegetation. This process also flips the leaves, improving the deposition of droplets on the undersides and lower-middle regions of the leaves [11]. Collectively, these technologies aim to optimize pesticide usage by increasing the coverage of the pesticide solution. Additionally, machine learning and targeted spraying systems can enable the automatic online classification and identification of target crops and weeds by integrating crop data with visual technology, thus enhancing the precision of pesticide application on designated crops [12]. However, the implementation of such systems often requires a high degree of freedom spraying actuators, such as robotic arms [13], which can complicate operations and increase costs. In contrast, adjustable linkages provide a wider range of application scenarios compared to robotic arms [14,15].

The linkage mechanism is a system composed of several interconnected links connected by joints. It is commonly used to facilitate complex motion trajectories that generate dynamic characteristics [16,17]. This mechanism demonstrates a variety of motion modes, allowing it to execute rotations, oscillations, translations, and complex movements within either a planar or three-dimensional environment. Such versatility facilitates the implementation of established motion laws and predetermined trajectories. Additionally, by modifying the number and length of the linkages, the mechanism can generate a wide range of output types [18,19]. This adaptability permits the linkage mechanism to conform to various application contexts and specifications [20]. The primary design methodologies for linkage structures include graphical methods [21], analytical methods [22], and numerical methods [23]. These approaches generally impose constraints on the parameters of the linkage mechanism by considering the positions of the target points along the trajectory of the output end [24,25]. However, the speed and acceleration of the output end are often overlooked, complicating the design and implementation of the linkage mechanism. After the design phase, it is typically necessary to analyze and verify the mechanism's dynamic characteristics [26]. If these characteristics do not meet the established design criteria, it may be necessary to optimize the parameters or, in some cases, undertake a comprehensive redesign of the mechanism. Therefore, the linkage mechanism frequently encounters the issue of inconsistent output speed in practical applications. When integrated with the spraying system, this inconsistency results in significant variations in the coverage of the spraying equipment across different areas of the crops. Such disparities not only hinder the effective utilization of pesticides but also challenge the comprehensive protection of the crops.

The control methodology employed for the linkage mechanism serves as a critical foundation for ensuring stable transmission. Traditional approaches predominantly utilize closed-loop control systems [13,27], in which sensors are integrated at the nozzle position to facilitate real-time monitoring and adjustment of the angular velocity of the spraying linkage. However, this control strategy is characterized by a certain degree of latency and involves a relatively complex system architecture. Closed-loop control is frequently employed in situations where the output load is substantial and continuously fluctuating. In the context of the linkage mechanism examined in this study, the variations in load at the output end of the linkage are minimal. Consequently, this study proposes an active control strategy for multi-linkage sprayers, which enables uniform adjustment of the spraying linkage angle. This innovation is anticipated to enhance the uniformity of spraying and contribute positively to the principles of ecological sustainability within the agricultural sector.

Based on the analysis presented above, the application of a linkage mechanism to a sprayer can collaboratively adjust the angle and position of the nozzles, demonstrating significant potential for comprehensive crop protection. However, multi-link mechanisms encounter the challenge of uneven output speeds in practical applications, which directly results in inconsistencies in the amount of spray delivered at different positions. To address this issue, this study aims to develop an active stability control method for a multi-link structure sprayer to enhance the uniformity of spraying. The research focuses on actively adjusting the output speed of the spraying equipment through precise mathematical modeling and the design of control strategies to achieve uniform application. The core of this method involves establishing a relationship model between input speed and output speed using differential equations, along with vector methods, implicit function transformation to explicit functions, and regression analysis, thereby providing a comprehensive solution that bridges theory and practice. This research not only presents a novel approach to resolving the existing challenges associated with multi-link spraying equipment, in alignment with global trends toward sustainable development and green ecological agriculture, but also serves as a reference for the stability control of other complex mechanical structures, showcasing significant application potential.

2. Materials and Methods

2.1. Structure and Principle of Multi-Link Spraying Machine

The research group has developed a spraying machine that precisely controls the position and angle of the nozzle through a linkage system. This design facilitates thorough spraying on the upper, lateral, and undersides of crop leaves. The primary structure is illustrated in Figure 1, which comprises a body frame, linkage mechanisms, medicine cabinets, walking wheels, and several additional components. The input point of the linkage mechanism is designated as point *A*, with power management facilitated by a ball screw. The nozzle is attached to link *DE*, which serves as the output of the linkage mechanism [28].

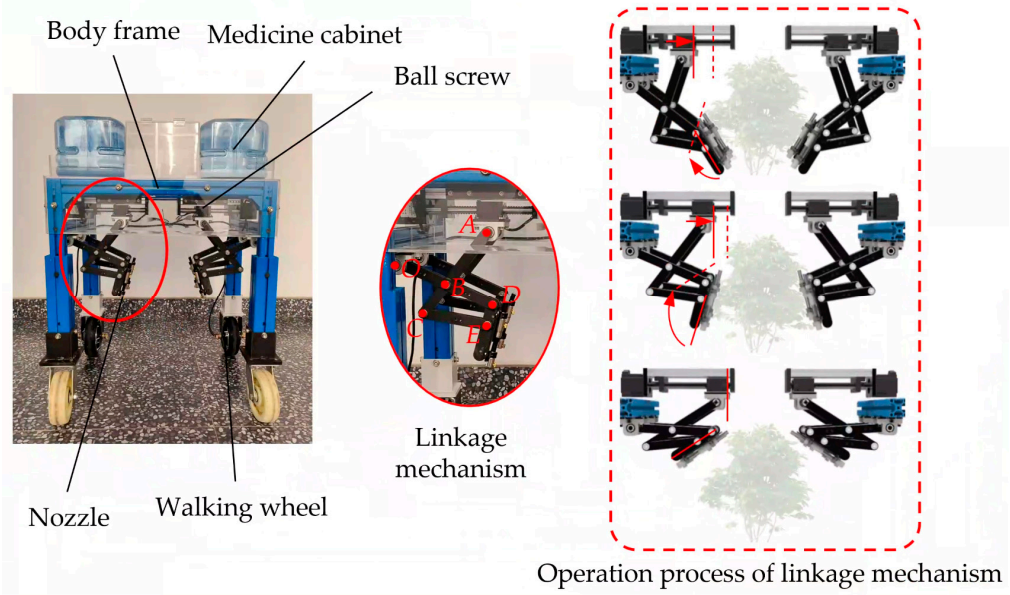


Figure 1. Configuration and operational principles of the multi-link mechanisms sprayer. Note: Points *O*, *A*, *B*, *C*, *D*, and *E* represent the hinge positions, while the arrows indicate the direction of motion.

When the drive motor of the ball screw operates at a constant velocity, the slider translates uniformly along the screw axis in conjunction with input point *A* of the linkage

mechanism. The interaction among various linkages results in continuous alterations in the position and angle of linkage *DE*, which, in turn, regulates the position and spray angle of the nozzle.

2.2. Modeling and Analysis of Linkage Mechanism

To establish the relationship between the input (position of slider *A*) and the output (nozzle connecting rod angle), a modeling analysis of the multi-link mechanisms was conducted. The fixed hinge point *O* of the linkage *OD* was designated as the origin of the coordinate system, with the horizontal axis oriented towards the crop defined as the *x*-axis and the vertical axis directed upwards from the ground defined as the *y*-axis. This configuration establishes a Cartesian coordinate framework, as illustrated in Figure 2. Following an initial design and optimization analysis, the dimensions of the connecting rods have been determined as follows: the length of the *OD* connecting rod is 184 mm (with the *OB* segment measuring 92 mm), the length of the *AC* connecting rod is 192 mm (with the *AB* segment measuring 120 mm), the length of the *CE* connecting rod is 120 mm, the length of the *DE* connecting rod is 40 mm, and the distance from point *O* to the screw axis is 57.5 mm [29].

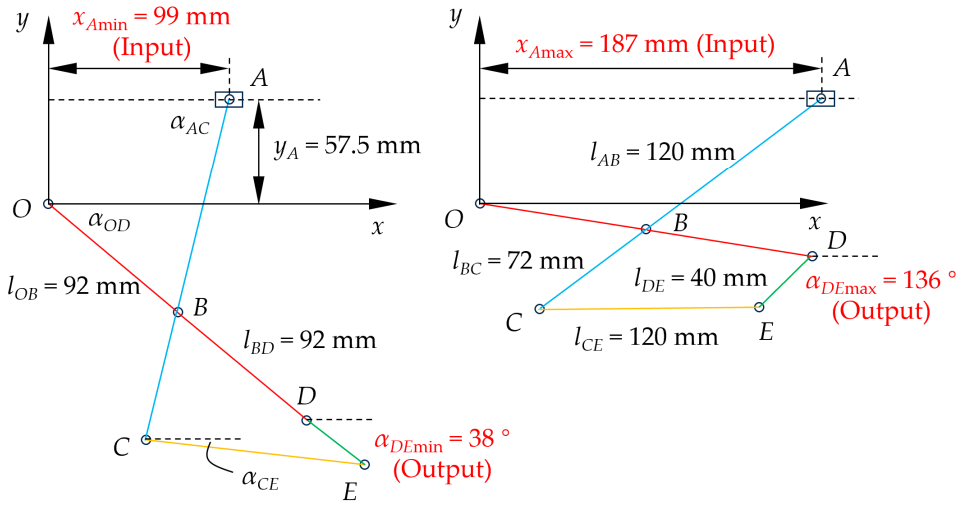


Figure 2. Modeling and analysis of multi-link mechanisms.

In order to clarify the functional relationship between the input and output variables of the linkage mechanism, a parametric modeling analysis of the linkage structure was conducted. First, the vector approach was utilized to derive the position equations for points *B* and *E* [29]:

$$\begin{cases} \mathbf{r_{OB}} = \mathbf{r_{OA}} + \mathbf{r_{AB}} \\ \mathbf{r_{BC}} + \mathbf{r_{CE}} = \mathbf{r_{BD}} + \mathbf{r_{DE}} \end{cases} \tag{1}$$

Note: $\mathbf{r_{OB}}$ represents the vector associated with the *OB*; $\mathbf{r_{OA}}$ denotes the vector corresponding to the *OA*; $\mathbf{r_{AB}}$ signifies the vector for the *AB*, $\mathbf{r_{BC}}$ indicates the vector related to the *BC*; $\mathbf{r_{CE}}$ refers to the vector of the *CE*; $\mathbf{r_{BD}}$ represents the vector pertaining to the *BD*; $\mathbf{r_{DE}}$ denotes the vector associated with the *DE*.

Through the application of orthogonal decomposition to Equation (1) in both the *x* and *y* directions, the following results were obtained:

$$\begin{cases} x_A - l_{AB}\cos\alpha_{AC} = l_{OB}\cos\alpha_{OD} \\ y_A - l_{AB}\sin\alpha_{AC} = -l_{OB}\sin\alpha_{OD} \\ x_C + l_{CE}\cos\alpha_{CE} = x_D + l_{DE}\cos\alpha_{DE} \\ y_C - l_{CE}\sin\alpha_{CE} = y_D - l_{DE}\sin\alpha_{DE} \end{cases} \tag{2}$$

In this context,

$$\begin{cases} x_C = x_A - l_{AC}\cos\alpha_{AC} \\ y_C = y_A - l_{AC}\sin\alpha_{AC} \\ x_D = l_{OD}\cos\alpha_{OD} \\ y_D = -l_{OD}\sin\alpha_{OD} \end{cases}$$

Note: (x_A, y_A) represents the coordinates of endpoint A in the xOy coordinate system, mm; (x_C, y_C) denotes the coordinates of endpoint C in the xOy coordinate system, mm; (x_D, y_D) indicates the coordinates of endpoint D in the xOy coordinate system, mm; l_{AB} refers to the length of the AB connecting rod, mm; l_{OB} is the length of the OB connecting rod, mm; l_{CE} represents the length of the CE connecting rod, mm; l_{DE} denotes the length of the DE connecting rod, mm; l_{AC} indicates the length of the AC connecting rod, mm; l_{OD} refers to the length of the OD connecting rod, mm; α_{AC} is the angle between the AC connecting rod and x-negative direction, °; α_{OD} is the angle between the OD connecting rod and the positive x-direction, °; α_{CE} is the angle between the CE connecting rod and the positive x-direction, °; α_{DE} is the angle between the DE connecting rod and the positive x-direction, °.

By integrating Equation (2), the correlation between the lateral displacement position x_A of the slider at point A and the angles α_{AC}, α_{OD}, and α_{DE} were derived.

$$\begin{cases} (x_A - l_{AB}cosa_{AC})^2 + (y_A - l_{AB}sina_{AC})^2 = {l_{OB}}^2 \\ (x_A - l_{OB}cosa_{OD})^2 + (y_A - l_{OB}sina_{OD})^2 = {l_{AB}}^2 \\ (x_D - x_c + l_{DE}cosa_{DE})^2 + (y_C - y_D + l_{DE}sina_{DE})^2 = {l_{CE}}^2 \end{cases} \quad (3)$$

2.3. Establishing Explicit Function Equations and Curve Fitting

In Equation (3), the lengths of each rod and the vertical coordinate y_A of point A are defined parameters. The angles corresponding to rods AC, OD, and CE exhibit a nonlinear relationship with respect to x_A. However, Equation (3) represents an implicit function, which complicates the calculation of the derivative of the functional relationship between the input speed v_A and the output speed ω_{DE}. Therefore, to isolate the independent variable x_A and the dependent variable α_{DE} in the implicit function equation, it is essential to conduct nonlinear fitting on the three implicit function equations presented in Equation (3) to transform them into explicit functions [30,31]. The objective is to achieve a coefficient of determination greater than 0.99, which will facilitate the identification of the highest degree of the fitting equation. The computational approach is illustrated in Figure 3, and the resulting data are presented in Table 1.

Table 1. Fitting results of explicit function equation..

Fitting Equations	Parameters	Value
$f(x_A) = A_4{x_A}^4 + A_3\,{x_A}^3 + A_2\,{x_A}^2 + A_1\,x_A + A_0$	A_4	-2.826×10^{-7}
	A_3	1.401×10^{-4}
	A_2	-2.591×10^{-2}
	A_1	1.711
	A_0	52.165
	R^2	0.999

Table 1. *Cont.*

Fitting Equations	Parameters	Value
$g(x_A) = B_5 {x_A}^5 + B_4 {x_A}^4 + B_3 {x_A}^3 + B_2 {x_A}^2 + B_1 x_A + B_0$	B_5	-7.202×10^{-9}
	B_4	4.825×10^{-6}
	B_3	-1.283×10^{-3}
	B_2	0.167
	B_1	−10.847
	B_0	323.539
	R^2	0.999
$h(x_A) = C_3 {x_A}^3 + C_2 {x_A}^2 + C_1 x_A + C_0$	C_3	1.425×10^{-4}
	C_2	-6.355×10^{-2}
	C_1	10.302
	C_0	−499.772
	R^2	0.999

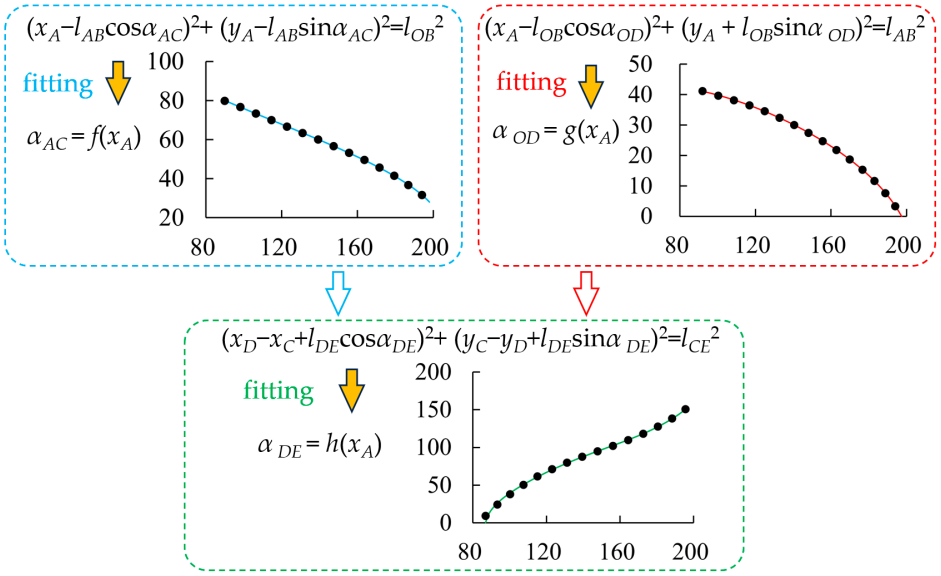


Figure 3. Explicit function equation and fitting process.

To establish the relationship between the velocity of slider and the angular velocity of the nozzle connecting rod, it is necessary to compute the derivative of the fitting equation $h(x_A)$ with respect to both x_A and α_{DE}.

$$\omega_{DE} = \left(3C_3 {x_A}^2 + 2C_2 x_A + C_1\right) v_A \tag{4}$$

Note: v_A represents the velocity of slider A, mm/s; ω_{DE} denotes the angular velocity of the nozzle connecting rod, °/s. C_1, C_2, and C_3 are fitting parameters, with their values detailed in Table 1.

2.4. Verification of Consistency Between Simulink and Adams Models

Utilizing the MATLAB Simulink R2018a module to address Equation (4) [32,33], and based on the structural analysis of the device, it is observed that when the horizontal coordinate x_A of the slider in the ball screw varies between 99 mm and 187 mm, the corresponding range of rotation angles for the spraying connecting rod DE spans from 38° to 136°.

The multi-link angle spraying machine discussed in this study is specifically designed for greenhouse planting environments. In contrast to large-scale outdoor farmland, greenhouse planting allows for precise control over environmental factors such as temperature,

humidity, and light, thereby creating optimal growth conditions for crops. However, the relatively enclosed nature of greenhouses also creates favorable air and soil conditions that can promote the survival and reproduction of pests and diseases. Consequently, the effective utilization of pesticides and the precision of spraying are more critical than operational efficiency [13,34]. Preliminary research indicates that if the speed of the linkage mechanism is excessively fast, it can lead to pesticide drift and negatively impact the dynamic characteristics of the mechanism. Therefore, this study examines single run times of 2, 3, and 4 s as examples, sacrificing some operational efficiency to achieve more effective spraying results. Based on the rotation angles of rod *DE* and single run time, the v_A values were calculated to be 44.0, 29.3, and 22.0 mm/s. The graphical representation and results are depicted in Figure 4, which demonstrates the temporal variation of the angular velocity ω_{DE} of the spraying connecting rod *DE* with time under different parameters. The angular velocity of the connecting rod *DE* exhibits a pattern of initial decline followed by an increase, reaching a maximum speed of approximately $1.91 \times v_A$ °/s at $t = 0$, and a minimum speed of about $0.86 \times v_A$ °/s at $t = 49.7/v_A$ s.

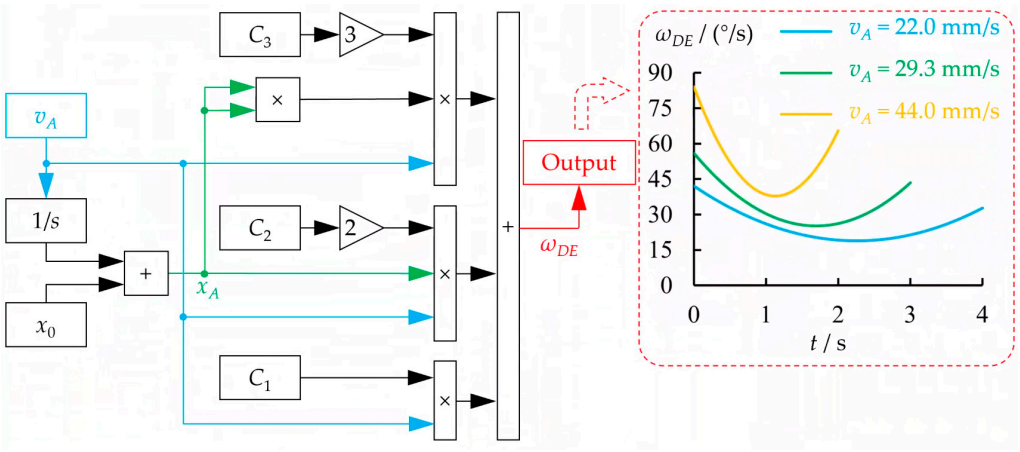


Figure 4. Model and outcomes of the ω_{DE} solver utilizing Simulink.

To validate the accuracy of the solution model, the dynamic analysis software Adams 2018 was employed to simulate the motion characteristics of the multi-link mechanisms [35,36]. SolidWorks was utilized to effectively simplify the ball screw and multi-link mechanisms by omitting minor components, such as bolts, that do not significantly influence the simulation outcomes. The resulting simplified model was subsequently imported into Adams, and constraints, drives, and marking points were reasonably added. The ball screw utilized in this investigation has a lead of 10 mm. Taking a running time of 3 s as an example, when the velocity v_A was set at 29.3 mm/s, the corresponding motor speed generated by the ball screw was calculated to be 175.8 r/min. Utilizing this information, the drive parameters were established, and the variation curve of the output value ω_{DE} of the multi-link mechanism is illustrated in Figure 5. A comparative analysis of the simulation outcomes from Simulink and those from Adams reveals that the trends and inflection points of both curves are largely congruent, thereby affirming the validity of the theoretical model and the results derived from Simulink.

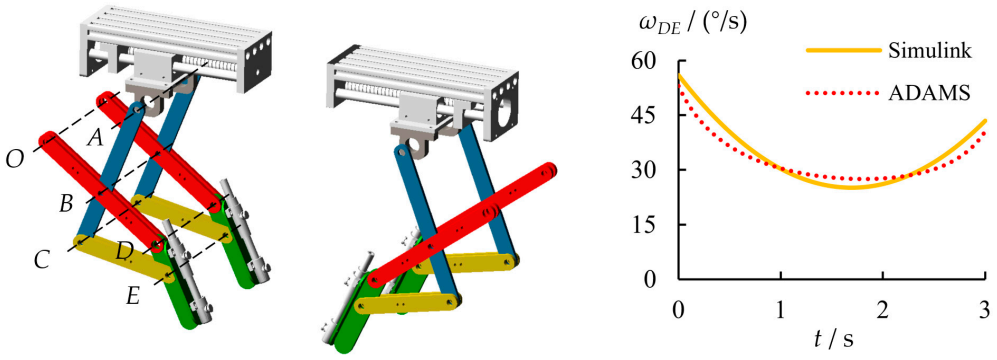


Figure 5. Adams model and Simulink simulation results. Note: *O*, *A*, *B*, *C*, *D*, and *E* represent the positions of the hinge pivot axis.

2.5. Solving Input Functions Based on Simulink

As illustrated in Figure 4, when the slider moves at a constant speed, the angular velocity of connecting rod *DE* exhibits non-uniformity. This variation leads to differences in the concentration of the pesticide solution being sprayed at various positions during actual spraying operations. To achieve a uniform and stable application of the pesticide solution, a reverse correction of the driving characteristics at the moving end was implemented. This process involves the active adjustment of v_A, which is assigned a nonlinear variation, thereby ensuring that the angular velocity of the nozzle mounting rod *DE* remains constant. The Simulink model corresponding to Equation (4) has been revised and constructed, with the nozzle angle adjustment range established between 38° and 136°. Based on simulation durations of 2, 3, and 4 s, the angular velocity ω_{DE} of the connecting rod *DE* for the nozzle installation, maintained at a constant velocity, have been determined to be 49.0, 32.7, and 24.5°/s, respectively. The graphical representation of the model and the corresponding results are shown in Figure 6. When the target angular velocity of the connecting rod *DE* for the nozzle installation is held constant, the input speed v_A of the slider exhibits a pattern of initial increase followed by a decrease. The peak speed is approximately $1.17 \times \omega_{DE}$ mm/s, occurring at $t = 60.03/\omega_{DE}$ s.

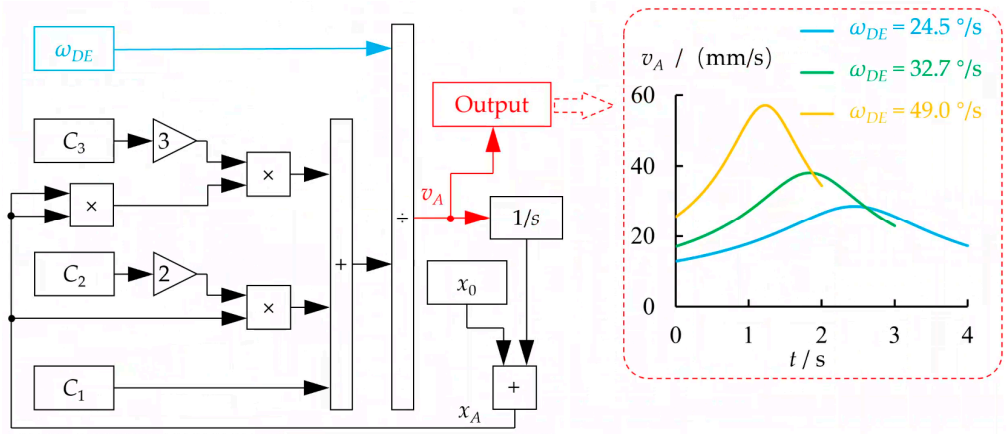


Figure 6. Model and outcomes of the v_A solver utilizing Simulink.

A polynomial representation of v_A, expressed as $v_A = \Sigma D_i t^i$, was developed based on the nonlinear input curve of v_A across various parameters. For clarity, a single runtime of 3 s was utilized to fit the variation curve of v_A, as depicted in Figure 7. To ensure a coefficient of determination exceeding 0.99 for the fitting equation, it was established that the polynomial must possess a minimum degree of 5. In order to fit the model to the target curve as closely as possible, the degree of the fitting equation was constrained to a range

between 5 and 9. The final results of the fitting process are presented in Table 2, indicating that uniform control at the output end can be theoretically attained.

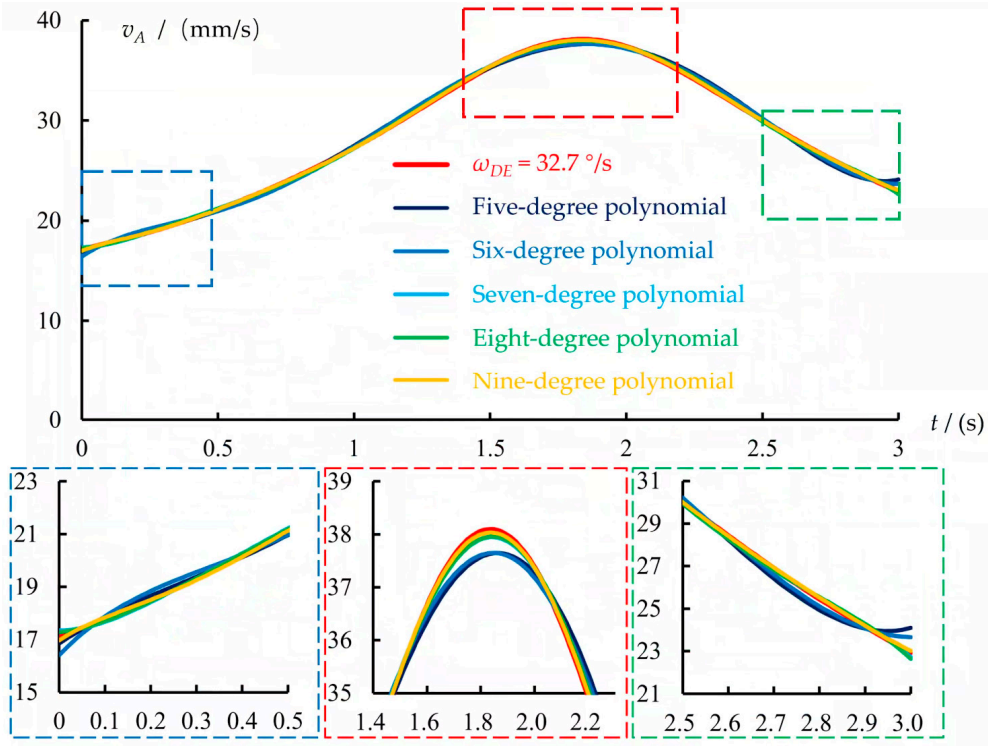


Figure 7. Fitting results at $\omega_{DE} = 32.7^{\circ}/\mathrm{s}$.

Table 2. Fitting results of different degree polynomial.

Parameters	Value				
	Five-Degree Polynomial	**Six-Degree Polynomial**	**Seven-Degree Polynomial**	**Eight-Degree Polynomial**	**Nine-Degree Polynomial**
D_9	/	/	/	/	0.849
D_8	/	/	/	−0.139	−11.603
D_7	/	/	−1.570	0.093	64.809
D_6	/	−0.583	15.899	7.757	−190.242
D_5	2.559	7.806	−60.622	−39.709	316.037
D_4	−16.703	−34.578	107.779	77.684	−302.248
D_3	32.561	61.109	−93.733	−69.758	162.730
D_2	−19.585	−40.908	42.205	32.477	−41.467
D_1	11.812	18.146	−0.071	1.567	11.420
D_0	16.848	16.411	17.343	17.279	16.974
R^2	0.99771	0.99812	0.99980	0.99981	0.99997

The motion characteristics of the output end of the linkage mechanism were validated using Adams, with the input end subjected to both constant speed (CS) and adjusted speed (AS) motions. When the velocity of the slider was input according to the fitting equation presented in Table 2, the variation curve of the output value ω_{DE} for the multi-link mechanism was illustrated in Figure 8. It is evident that, in comparison to the CS curve, the stability of the AS curves corresponding to different fitting intervals has improved. Nonetheless, due to inherent inaccuracies in the fitting equations, the AS curve continues to display minor fluctuations. The trends observed in the curves derived from various fitting intervals are generally consistent, with discrepancies primarily evident in the terminal data.

Notably, the AS curves resulting from the 5- and 7-degree polynomials exhibit reduced fluctuations at the end when compared to the 9-degree polynomial.

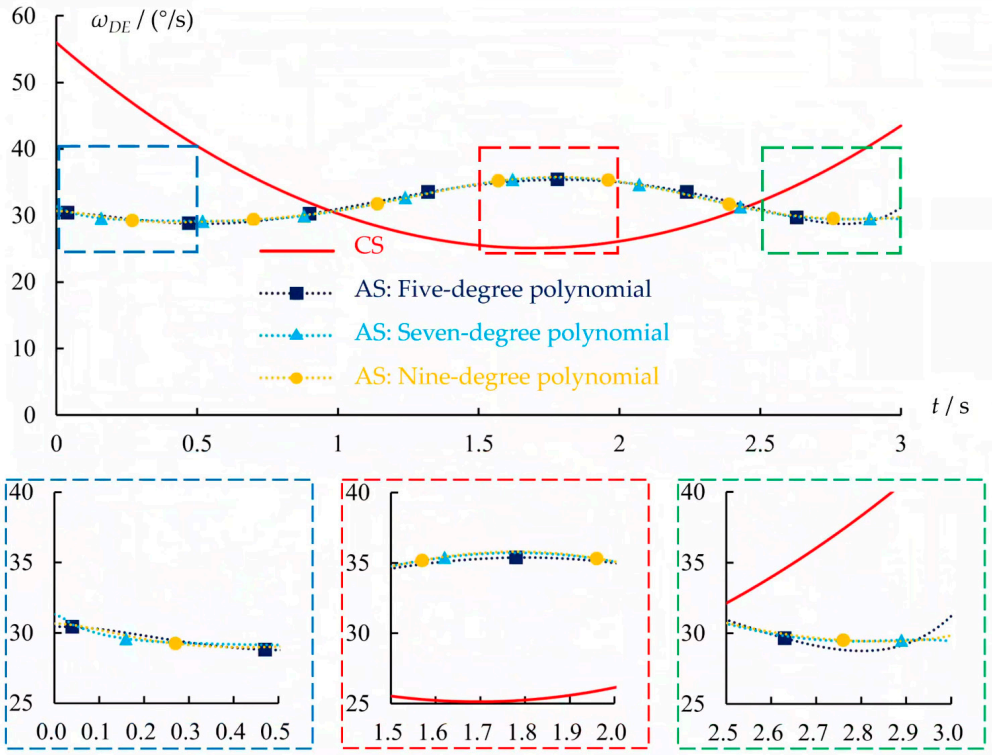


Figure 8. Simulation results of ω_{DE} output based on Adams.

3. Testing, Results, and Analysis

3.1. Testing Plan

To evaluate the motion response characteristics of the output end of the multi-link spraying mechanism, a series of comparative tests were conducted. The active control process and testing configuration are depicted in Figure 9. The input end of the multi-link spraying mechanism is driven by a motor through a ball screw with a screw pitch of 10 mm. The desired rotational speed of the motor for the tests is determined based on the speed and pitch of slider A, with control signals transmitted to the motor via an Arduino interface [37,38]. The rotation angle of the spraying connecting rod DE serves as the output terminal of the multi-link spraying mechanism. An electronic compass sensor was attached to the spraying connecting rod DE to measure the angular velocity at the output end, with a designated sampling interval of 0.1 s.

Using a target speed of ω_{DE} = 32.7°/s and a test duration of 3 s as a case study, the stepper motor was initially configured using the DM542 driver (manufactured by Wenzhou Pfede Electromechanical Co., Ltd. in Wenzhou, China) to ensure the accuracy of the feedback data during the testing process. First, a multimeter is used to measure and calibrate the input voltage of the driver to 24 V. Next, to ensure the accuracy of the Adams simulation and the consistency of the variables with the actual measured results, the input signal frequency is set to 0.01 s based on the Adams simulation step size. Finally, the motor input is regulated to operate in accordance with the control signals CS and AS. The speed-driving curve of the motor associated with AS was established using the 7-degree polynomial equation presented in Table 2. The relationship between motor speed and slider speed within the ball screw system is described by Equation (5).

$$n = \frac{v_A}{P} \times 60 \tag{5}$$

Note: n represents the rotational speed of the motor, r/min; P denotes the pitch of the ball screw, which is established at 10 mm in this study.

The rotation angle of the spray installation's connecting rod DE was determined through video recording. The data collected from the electronic compass sensor was then analyzed to validate the accuracy of the employed research methodology.

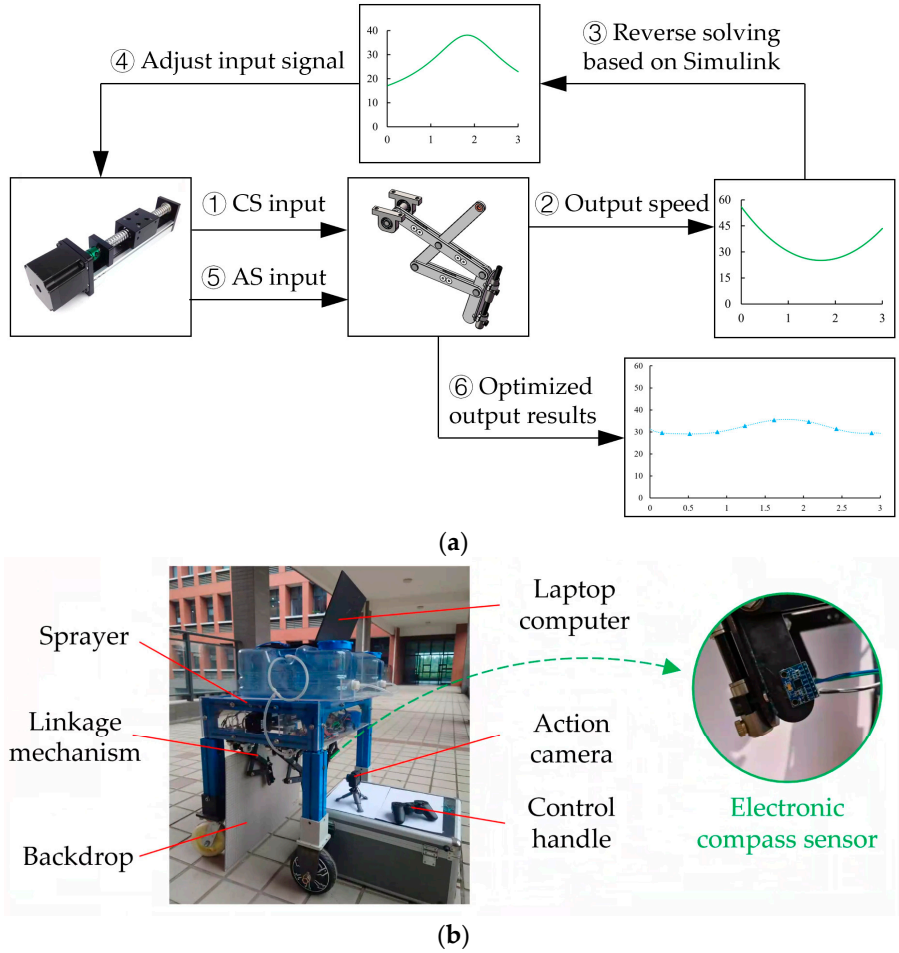


Figure 9. Schematic representation of testing layout: (**a**) active control process; (**b**) testing configuration.

3.2. Comparison and Analysis of Angular Velocity Between CS and AS

The test parameters of CS were that the driving motor operates at a constant speed of 175.8 r/min (corresponding to a slider speed of 29.3 mm/s). According to the fitting equation provided in Table 2 and Equation (5), AS drives the motor at variable speeds. Specifically, the driving equation is n= $(-1.570 \times t^7 + 15.899 \times t^6 - 60.622 \times t^5 + 107.779 \times t^4 - 93.733 \times t^3 + 42.205 \times t^2 - 0.071 \times t + 17.343) \times 60/10$. The resultant test outcomes are illustrated in Figure 10. Analysis reveals that the trend in angular velocity for the CS aligns closely with the results obtained from the Adams model and Simulink simulations depicted in Figure 5. The angular velocity variation trend of AS fluctuates in a small range within 27.8°/s to 36.7°/s. When compared to the CS, the AS demonstrates a marked enhancement in the stability of angular velocity at the output end of the linkage. Specifically, using a target speed of ω_{DE} = 32.7°/s as a reference, the output results of the AS demonstrate a maximum error of no more than 15.0%. This level of precision is comparable to that achieved by PID control, which exhibits a maximum error of no more than 15.8% [16], and it is accomplished without the need for additional sensors. This finding substantiates the viability of the active control methodology based on the linkage mechanism proposed in this research.

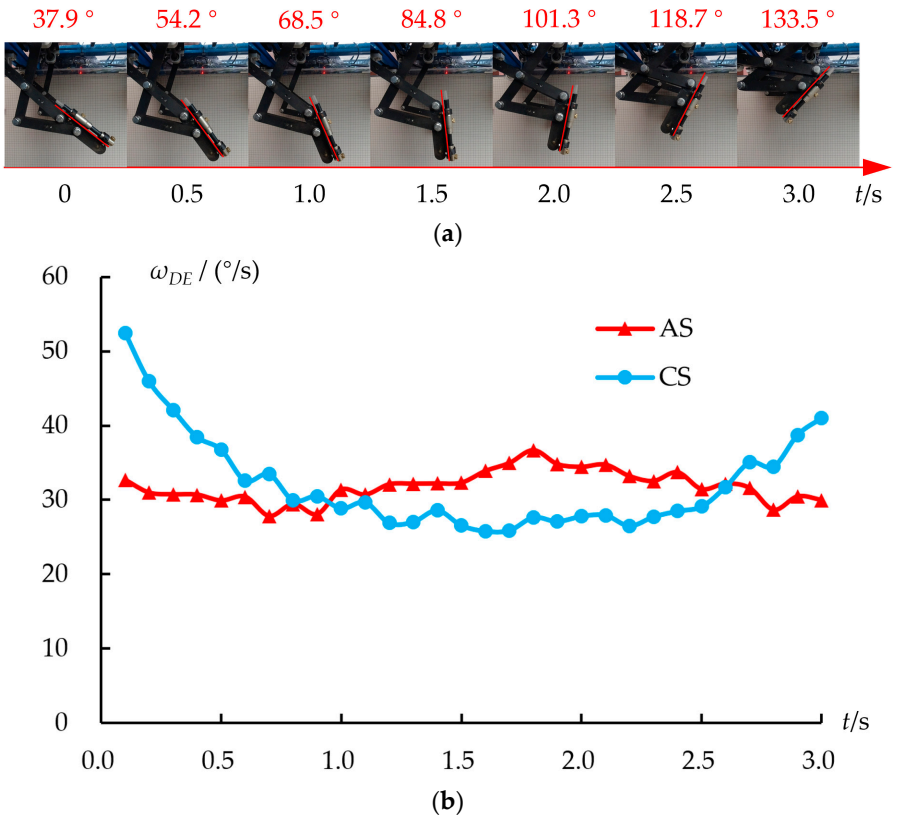


Figure 10. Resultant test outcomes: (**a**) angle results; (**b**) angular velocity results.

3.3. Comparison Test of Spraying with CS and AS

To evaluate the effectiveness of the active control method introduced in this research for improving the uniformity of spraying, a comparative test was conducted involving spraying operations. In this test, water was used in place of the spray mixture, and water-sensitive paper (WSP) was strategically positioned on the top, sides, and bottom of the crops. Upon completion of the test, immediate scanning was performed, and the droplet coverage rate was quantified using ImageJ software 1.38x. The results pertaining to the WSP and the coverage rate after testing are presented in Figure 11.

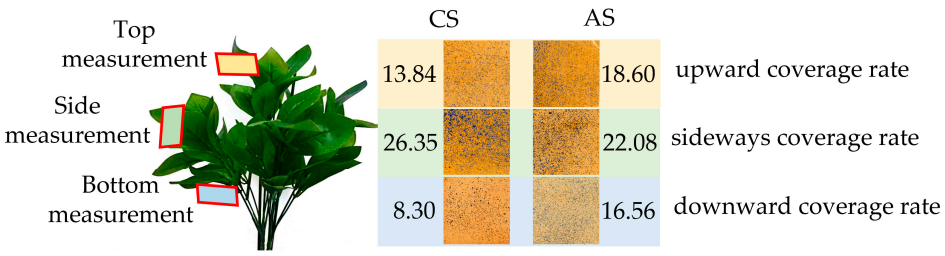


Figure 11. Spraying test results of CS and AS.

The data indicate that for CS, the sideways spray coverage rate of crops is significantly greater than that of the upward and downward positions, exhibiting a range of 18.05% across the three orientations. This trend is similar to the results obtained in the experiments of reference [15]. The specific coverage rates are 66.78% for the top layer, 74.39% for the middle layer, and 71.72% for the substratum. The key difference is that reference [15] employed fixed-angle spraying on the sides of the crops, where the coverage rate at various positions primarily depends on the diffusion of the droplets. In this study, the discrepancy can primarily be attributed to the uneven angular velocity at the output end of the linkage mechanism. As illustrated in Figure 4, the pattern of variation in ω_{DE} initially decreases

before subsequently increasing, which extends the duration of spraying on the sides of the crops. Given a constant spraying volume per unit time, the amount of water applied is positively correlated with the duration of spraying. Consequently, the coverage rate of water on the sides is the highest. Furthermore, it can be inferred that the coverage rate on the upward of the crops is marginally greater than that on the downward.

In comparison to the coverage results of CS, AS resulted in a significant reduction in coverage on the sideways of the crops, while simultaneously enhancing coverage on both the upward and downward surfaces. The optimized coverage range for the three positions is 5.52%. Compared to spraying at various angles with a fixed nozzle position [11], the difference in coverage across different positions is 9.15%; this study effectively minimizes the extreme variance in spray distribution. Compared to spraying systems equipped with visual and other sensors, the elimination of various sensor configurations [7] and the simplification of motor control complexity due to multiple degrees of freedom [13] can significantly improve the control of the mechanism and enhance the cost effectiveness of the sensors.

However, it is important to note that the coverage on the upward, sideways, and downward surfaces does not achieve complete uniformity. This discrepancy can be attributed to three primary factors: first, following the ejection of droplets from the nozzle, they must navigate through drift and diffusion to reach the leaf surface. During this transit, the droplets are significantly influenced by gravity, which complicates their adherence to the downward of the leaf, thereby resulting in a diminished coverage rate on that surface. Second, despite achieving a correlation coefficient of 0.99 in the curve-fitting process, minor discrepancies persist, particularly in proximity to the initial point. These discrepancies contribute to slight variations in the final angular velocity of the linkage movement. Third, the motion trajectory of the output end of the linkage mechanism developed in this study is characterized by a complex composite motion that combines both parallel and circular movements, rather than a straightforward circular motion. Consequently, when the output linkage operates at a constant angular velocity, the actual distribution density of the liquid diffusion is not entirely uniform.

4. Conclusions and Further Work

This study investigates the variable speed characteristics at the output end of a linkage mechanism and introduces an active control strategy. The proposed method involves dynamically adjusting the control equations governing the input variables to facilitate uniform motion at the output end. Utilizing a multi-link mechanism sprayer as a case study, the research formulates a fitting equation that relates the input and output variables within the multi-link mechanisms through a process of vector equation establishment and implicit function manifestation. The equation is subsequently solved using the MATLAB Simulink module, resulting in an analytical expression for the input variables that maintains a stable angular velocity of the output link within a specific linkage mechanism. Dynamic analysis conducted with Adams software revealed that the stability of the AS curve is significantly enhanced compared to the CS curve, thereby substantiating the efficacy of the methodologies employed in this research.

The findings from the dynamic analysis of the linkage mechanism, conducted using a testing prototype, reveal that within a single operational cycle of 3 s (equivalent to an angular velocity of ω_{DE} = 32.7°/s), the observed angular velocity profiles for both the CS and the AS align closely with the analytical predictions. Specifically, the angular velocity of the CS ranges from 25.8°/s to 52.5°/s, while the angular velocity of the AS exhibits minor fluctuations within a narrow band of 27.8°/s to 36.7°/s. This observation indicates that the speed-regulated linkage mechanism effectively contributes to the stabilization of the output

angular velocity. Therefore, these results substantiate the feasibility of employing the proposed active control method based on the linkage mechanism in practical applications.

From the perspective of actual spraying efficacy, the operational stability of the AS significantly surpasses that of the CS. The variability in the spraying coverage rate across the upward, sideways, and downward of the leaves has been reduced from 18.05% to 5.52%. However, it is important to note that the coverage across the three positions of the AS nozzle is not entirely uniform. Specifically, the coverage on the sideways of the leaf is comparatively greater, while the coverage on the underside is relatively lesser. This variation can be attributed to the combined effects of gravitational droplet diffusion and the complex motion dynamics of the linkage mechanism. Therefore, for the multi-link mechanism sprayer proposed in this study, maintaining a constant angular velocity at the output end can significantly improve the uniformity of spraying; however, this approach does not represent the optimal solution. The ideal angular velocity–time profile should be determined based on the distribution density of the spray mixture solution diffusion, which will guide the optimization of the input variable curve. More generally, the methodology presented in this study is applicable to any linkage mechanism where there exists a unique correspondence between input and output variables. Furthermore, in specific scenarios where the output variable must conform to a particular dynamic equation, the proposed method remains applicable, provided it aligns with the adjustment of the input parameters of the Simulink solving model. This approach also outlines the direction for the future optimization of multi-link spraying machines.

Author Contributions: Conceptualization, N.S. and Y.Y.; methodology, H.L. and N.S.; software, H.H. and J.Y.; validation, Z.C. and T.X.; writing—original draft preparation, N.S. and H.L.; writing—review and editing, N.S. and Y.Y.; project administration, N.S. and H.L. All authors have read and agreed to the published version of the manuscript.

Funding: This research was funded by the National Natural Science Foundation of China (Grant No. 32201673), the China Postdoctoral Science Foundation (Grant No. 2023M741436), the Natural Science Foundation of the Jiangsu Higher Education Institutions of China (Grant No. 23KJB630001), the Science and Technology Plan Project of Changzhou (Grant No. CQ20220082).

Institutional Review Board Statement: Not applicable.

Informed Consent Statement: Not applicable.

Data Availability Statement: The raw data supporting the conclusions of this article will be made available by the authors on request.

Conflicts of Interest: The authors declare no conflicts of interest.

References

1. Cantelli, L.; Bonaccorso, F.; Longo, D.; Melita, C.D.; Schillaci, G.; Muscato, G. A small versatile electrical robot for autonomous spraying in agriculture. *AgriEngineering* **2019**, *1*, 391–402. [CrossRef]
2. Meshram, A.T.; Vanalkar, A.V.; Kalambe, K.B.; Badar, A.M. Pesticide spraying robot for precision agriculture: A categorical literature review and future trends. *J. Field Robot.* **2022**, *39*, 153–171. [CrossRef]
3. Abbas, I.; Liu, J.; Faheem, M.; Noor, R.S.; Shaikh, S.A.; Solangi, K.A.; Raza, S.M. Different sensor based intelligent spraying systems in Agriculture. *Sens. Actuators A Phys.* **2020**, *316*, 112265. [CrossRef]
4. Zanin, A.R.A.; Neves, D.C.; Teodoro, L.P.R.; Silva Júnior, C.A.; Silva, S.P.; Teodoro, P.E.; Baio, F.H.R. Reduction of pesticide application via real-time precision spraying. *Sci. Rep.* **2022**, *12*, 5638. [CrossRef] [PubMed]
5. Amaya, K.; Bayat, A. Innovating an electrostatic charging unit with an insulated induction electrode for air-assisted orchard sprayers. *Crop Prot.* **2024**, *181*, 106701. [CrossRef]
6. Wei, Z.; Li, R.; Xue, X.; Sun, Y.; Zhang, S.; Li, Q.; Chang, C.; Zhang, Z.; Sun, Y.; Dou, Q. Research status, methods and prospects of air-assisted spray technology. *Agronomy* **2023**, *13*, 1407. [CrossRef]

7. Hussain, N.; Farooque, A.A.; Schumann, A.W.; McKenzie-Gopsill, A.; Esau, T.; Abbas, F.; Acharya, B.; Zaman, Q. Design and development of a smart variable rate sprayer using deep learning. *Remote Sens.* **2020**, *12*, 4091. [CrossRef]
8. Cui, L.F.; Xue, X.Y.; Ding, S.M.; Le, F.X. Development of a DSP-based electronic control system for the active spray boom suspension. *Comput. Electron. Agric.* **2019**, *166*, 105024. [CrossRef]
9. Li, J.Y.; Nie, Z.Y.; Chen, Y.F.; Ge, D.Q.; Li, M.Q. Development of boom posture adjustment and control system for wide spray boom. *Agriculture* **2023**, *13*, 2162. [CrossRef]
10. Appah, S.; Wang, P.; Ou, M.; Gong, C.; Jia, W. Review of electrostatic system parameters, charged droplets characteristics and substrate impact behavior from pesticides spraying. *Int. J. Agric. Biol. Eng.* **2019**, *12*, 1–9. [CrossRef]
11. Dai, S.Q.; Ou, M.X.; Du, W.T.; Yang, X.J.; Dong, X.; Jiang, L.; Zhang, T.; Ding, S.M.; Jia, W.D. Effects of sprayer speed, spray distance, and nozzle arrangement angle on low-flow air-assisted spray deposition. *Front. Plant Sci.* **2023**, *14*, 1184244. [CrossRef] [PubMed]
12. Alam, M.; Alam, M.S.; Roman, M.; Tufail, M.; Khan, M.U.; Khan, M.T. Real-time machine-learning based crop/weed detection and classification for variable-rate spraying in precision agriculture. In Proceedings of the 2020 7th international conference on electrical and electronics engineering (ICEEE), Antalya, Turkey, 14–16 April 2020; pp. 273–280.
13. Hejazipoor, H.; Massah, J.; Soryani, M.; Vakilian, K.A.; Chegini, G. An intelligent spraying robot based on plant bulk volume. *Comput. Electron. Agric.* **2021**, *180*, 105859. [CrossRef]
14. Liu, X.M.; Li, Y.; Li, M.; Yuan, J.; Fang, Q.Z.; Hou, J.L. Design and test of smart-targeting spraying system on boom sprayer. *Trans. Chin. Soc. Agric. Mach.* **2016**, *47*, 37–44.
15. Luo, Y.H.; Huang, D.F.; Jiang, P.; Xiang, S.L.; Liu, J.F.; Xu, M.Z.; Shi, Y.X. Design and experimental testing of an overhead rail automatic variable-distance targeted spray system for solar greenhouses. *Agriculture* **2023**, *13*, 1853. [CrossRef]
16. Chen, Z.H.; Wang, S.K.; Liu, Q.; Wang, J.Z. Development of sheet palletizing manipulator based on multi-link mechanism. *Res. Sq.* **2020**.
17. Wei, G.W.; Dai, J.S. A spatial eight-bar linkage and its association with the deployable platonic mechanisms. *J. Mech. Robot.* **2014**, *6*, 021010. [CrossRef]
18. Zhang, Y.H.; Zhang, L.F.; Wang, W.; Li, Y.M.; Zhang, Q.W. Design and implementation of a two-wheel and hopping robot with a linkage mechanism. *IEEE Access* **2018**, *6*, 42422–42430. [CrossRef]
19. Kim, J.W.; Seo, T.; Kim, J. A new design methodology for four-bar linkage mechanisms based on derivations of coupler curve. *Mech. Mach. Theory* **2016**, *100*, 138–154. [CrossRef]
20. Lin, H.K.; Tekes, A.; Tekes, C. Design, development and modelling of single actuated, compliant and symmetrical multilink hopping mechanism. *J. Mech. Sci. Technol.* **2020**, *34*, 555–563. [CrossRef]
21. Huang, T.C.; Youm, Y. Exact displacement analysis of four-link spatial mechanisms by the direction cosine matrix method. *J. Appl. Mech.* **1984**, *51*, 921–928. [CrossRef]
22. Liu, Y.W.; Wang, H.G.; Li, B.; Zhou, W.J. An optimal method to determine the parameters of anthropomorphic finger based on four-link mechanism. In Proceedings of the 2008 2nd IEEE RAS & EMBS International Conference on Biomedical Robotics and Biomechatronics, Scottsdale, AZ, USA, 19–22 October 2008; IEEE: Piscataway, NJ, USA; pp. 842–847.
23. Martini, A.; Troncossi, M.; Carricato, M.; Rivola, A. Elastodynamic behavior of balanced closed-loop mechanisms: Numerical analysis of a four-bar linkage. *Meccanica* **2014**, *49*, 601–614. [CrossRef]
24. Muralidharan, V.; Bose, A.; Chatra, K.; Bandyopadhyay, S. Methods for dimensional design of parallel manipulators for optimal dynamic performance over a given safe working zone. *Mech. Mach. Theory* **2020**, *147*, 103721. [CrossRef]
25. Lee, S.; Kim, J.; Kang, N. Deep generative model-based synthesis framework of four-bar linkage mechanisms with target conditions. *J. Comput. Des. Eng.* **2024**, *11*, 318–332. [CrossRef]
26. Chen, H.C.; Liu, T.K.; Huang, I.M.; Chou, J.H. Multiobjective synthesis of six-bar mechanisms under manufacturing and collision-free constraints. *IEEE Comput. Intell. Mag.* **2012**, *7*, 36–48. [CrossRef]
27. Allmendinger, A.; Spaeth, M.; Saile, M.; Peteinatos, G.G.; Gerhards, R. Precision chemical weed management strategies: A review and a design of a new CNN-based modular spot sprayer. *Agronomy* **2022**, *12*, 1620. [CrossRef]
28. Shi, N.Y.; Chen, Z.; Li, H.; Hua, H.L.; Xu, T.; Ye, J.H. Development and assessment of a novel single-drive variable angle spraying machine. *Sci. Rep.* **2024**, *14*, 31264. [CrossRef] [PubMed]
29. Sinir, B.G. Derivation of governing equations by using vector approach and comparison of analytical solutions of post-buckling behaviors of transverse functionally graded shear deformable beam theories. *Arab. J. Sci. Eng.* **2023**, *48*, 4971–4990. [CrossRef]
30. Corduneanu, E. Expressions of euler angles as functions of the directional cosines of three-orthogonal axes in rigid body kinematics-II. *Bull. Polytech. Inst. Iași. Mach. Constr. Sect.* **2021**, *67*, 17–24. [CrossRef]
31. Wang, W.J. The explicit expression of axis and angle of a rotation matrix. *Coll. Math. J.* **2021**, *52*, 39–44. [CrossRef]
32. Zhang, W.N.; Zhong, S.; Xia, Y.; Xu, D.W. Air vehicle's attitude control system based on virtual instrument. In Proceedings of the 2007 8th International Conference on Electronic Measurement and Instruments, Xi'an, China, 16–18 August 2007; pp. 3–74.

33. Ponomarev, A.; Hofmann, J.; Groll, L. Characteristics-based Simulink implementation of first-order quasilinear partial differential equations. In Proceedings of the 10th International Conference on Simulation and Modeling Methodologies, Online, 8–10 July 2020; Volume 1907, p. 13419.
34. Sánchez-Hermosilla, J.; Rincón, V.J.; Páez, F.; Agüera, F.; Carvajal, F. Field evaluation of a self-propelled sprayer and effects of the application rate on spray deposition and losses to the ground in greenhouse tomato crops. *Pest Manag. Sci.* **2011**, *67*, 942–947. [CrossRef] [PubMed]
35. Xiao, Y.H.; Wang, J.R.; Yang, J.Q.; Li, J. Dynamic simulation research of adaptive support mechanism of pipeline inspection robot based on ADAMS. *J. Phys. Conf. Ser.* **2023**, *2450*, 012047. [CrossRef]
36. Šarga, P.; Hroncová, D.; Rákay, R. The MSC ADAMS/view and simulation of the crank rocker mechanism. *Am. J. Mech. Eng.* **2015**, *3*, 161–164.
37. Shi, N.Y.; Li, H.; Xu, T.; Hua, H.L.; Ye, J.H.; Chen, Z. Design, analysis, and optimization testing of a novel modular walking device for pipeline robots. *Machines* **2024**, *12*, 718. [CrossRef]
38. Flores-Campos, J.A.; Perrusquía, A.; Hernández-Gómez, L.H.; González, N.; Armenta-Molina, A. Constant speed control of slider-crank mechanisms: A joint-task space hybrid control approach. *IEEE Access* **2021**, *9*, 65676–65687. [CrossRef]

Disclaimer/Publisher's Note: The statements, opinions and data contained in all publications are solely those of the individual author(s) and contributor(s) and not of MDPI and/or the editor(s). MDPI and/or the editor(s) disclaim responsibility for any injury to people or property resulting from any ideas, methods, instructions or products referred to in the content.